ASSESSING THE PEATLAND HUMMOCK-HOLLOW CLASSIFICATION FRAMEWORK USING HIGH-RESOLUTION ELEVATION MODELS: IMPLICATIONS FOR APPROPRIATE COMPLEXITY ECOSYSTEM MODELLING

Paul A. Moore[1*], Maxwell C. Lukenbach[1], Dan K. Thompson[2], Nick Kettridge[3], Gustaf Granath[4], and James M. Waddington[1]

[1] School of Geography and Earth Sciences, McMaster University,1280 Main Street West, Hamilton, ON, L8S 4K1, Canada

[2] Northern Forestry Centre, Canadian Forest Service, Natural Resources Canada, Edmonton, Alberta, AB, T6H 3S5, Canada

[3] School of Geography, Earth and Environmental Sciences, University of Birmingham, Edgbaston, Birmingham, B15 2TT, United Kingdom.

[4] Department of Ecology and Genetics, Uppsala University, Norbyvägen 18D, 736 52 Uppsala, Sweden

* Corresponding author: Paul Moore (paul.moore82@gmail.com)

Manuscript for submission to Biogeosciences

KEY WORDS: microtopography, morphometry, sampling design, structure from motion, mire

ABSTRACT

The hummock-hollow classification framework used to categorize peatland ecosystem microtopography is pervasive throughout peatland experimental designs and current peatland ecosystem modelling approaches. However, identifying what constitutes a representative hummock-hollow pair within a site and characterizing hummock-hollow variability within or between peatlands remains largely unassessed. Using structure-from-motion (SfM), high resolution digital elevation models (DEM) of hummock-hollow microtopography were used to: 1) examine how much area needs to be sampled to characterize site-level microtopographic variation; and 2) examine the potential role of microtopographic shape/structure on biogeochemical fluxes using plot-level data from 9 northern peatlands. To capture 95% of site-level microtopographic variability, on average an aggregate sampling area of 32 m^2 composed of ten randomly located plots was required. Both site- (*i.e.* transect data) and plot-level (*i.e.* SfM-derived DEM) results show that microtopographic variability can be described as a fractal at the sub-metre scale, where contributions to total variance are very small below a 0.5 m length scale. Microtopography at the plot-level was often found to be non-bimodal, as assessed using a Gaussian mixture model (GMM). Our findings suggest that the non-bimodal distribution of microtopography at the plot-level may result in an under-sampling of intermediate topographic positions. Extended to the modelling domain, an under-representation of intermediate microtopographic positions is shown to lead to potentially large flux biases over a wide range of water table positions for ecosystem processes which are non-linearly related to water and energy availability at the moss surface. Moreover, our simple modelling results suggest that much of the bias can be eliminated by representing

45 microtopography with several classes rather than the traditional two (*i.e.*
46 hummock/hollow). A range of tools examined herein can be used to easily parameterize
47 peatland models, from GMMs used as simple transfer functions, to spatially explicit fractal
48 landscapes based on simple power law relations between microtopographic variability
49 and scale.
50
51 **INTRODUCTION**
52 Northern peatlands in the maritime-temperate, boreal, and subarctic have been persistent
53 terrestrial sinks for carbon throughout the Holocene, storing on the order of 500 Gt of
54 carbon as organic soil deposits (Yu, 2012). However, these peatland carbon stores are
55 now considered to be at risk from the effects of climate change due to warmer
56 temperatures and prolonged periods of drought which would increase carbon loss through
57 decomposition and increased wildfire consumption (Moore et al., 1998; Yu et al., 2009;
58 Turetsky et al., 2002; Kettridge et al., 2015). While these positive feedbacks cause carbon
59 loss (*e.g.* Ise et al., 2008; Blodau et al., 2004), the long-term stability of peatland carbon
60 may be maintained by negative ecohydrological feedbacks that promote resilience to
61 environmental change (Belyea and Clymo, 2001; Waddington et al., 2015; Hodgkins et
62 al., 2018). These negative feedbacks depend, in part, on the presence of
63 microtopography (microforms) that provides spatial diversity in ecohydrological structure
64 and biogeochemical function across a peatland (Belyea and Clymo, 2001; Belyea and
65 Malmer, 2004; Eppinga et al., 2008; Pedrotti et al., 2014; Malhotra et al., 2016).
66
67 Peatland microform classification is typically defined by their proximity to the water table

and characteristic vegetation assemblages, such as different species of *Sphagnum* moss and cover of woody shrubs (Andrus et al., 1983; Rydin and McDonald, 1985; Belyea and Clymo, 1998). Hummocks and hollows occur at a spatial scale of 1 to 10 m (S2 – Belyea and Baird, 2006), with hummocks typically covering an area of up to a few square metres. The hummock surface is typically located ~0.20 m or higher above the water table (Belyea and Clymo 1998; Malhotra et al., 2016). Hollows are closer to the water table and may occasionally be inundated, and 'lawns' are intermediate to hummocks and hollows (Belyea and Clymo, 1998).

Conceptualizing and qualitatively classifying complex peatland microtopography as hummocks and hollows is common in peatland research (*e.g.* Waddington and Roulet 1996; Belyea and Clymo 2001; Nungesser 2003; Benscoter et al., 2005; Bruland and Richardson 2005; Moser et al., 2007) as it is simple and allows for straightforward sampling designs, however, the visual characterization of hummocks and hollows is subjective and has the potential to produce biased results for several reasons. First, although microform vegetation and hydrology may be included in detailed study site/method descriptions, these characteristics may be quite different for microforms classified as hummocks at one study site compared to hummocks at a different study site. Biogeochemical function (ecosystem fluxes) may differ for microforms within a site (*e.g.* Bubier et al., 1993; Pelletier et al., 2011), but if the vegetation and hydrology of those microforms vary for different peatlands, assumptions for hummock and hollow biogeochemical function at one site may not be applicable to other peatlands. Given that there may also be large differences in the relative/absolute height and surface roughness

of microforms between sites, comparing studies with hummock and hollow microforms as a central component of the sampling design can be problematic. Moreover, the surface area, spatial distribution, and relative proportion of hummock and hollow microforms present within a peatland also vary between sites (*e.g.* Moore et al., 2015), which may introduce bias into sampling design. For example, researchers may over-sample the visually obvious extremes of the hummock-hollow continuum. Given that several peatland hydrological and ecosystem carbon models parameterize peat decomposition, production and hydraulic properties based on peatland microform classification (*e.g*. Cresto Aleina et al., 2015; Dimitrov et al., 2010; Sonnentag et al., 2008), the aforementioned sampling and classification biases may also lead to issues in determining the scale and complexity required for ecosystem modelling (*e.g.* Larsen et al., 2016).

The construction of a digital elevation model (DEM) in a peatland allows for the classification of microforms based on quantitative measures (*e.g.* relative position, slope, roughness) (*e.g.* Mercer and Westbrook, 2016; Rahman et al., 2017) rather than relying on qualitative/visual methods. Given the wide use and adoption of the hummock-hollow conceptual framework, we examine the potential utility of DEM quantitative techniques to overcome the concerns with the dominant qualitative hummock and hollow framework/classification scheme. As such, the two main objectives of this study were to: (i) provide a geostatistical/geospatial description of microtopographic variation in peatlands; and (ii) to use simple physically-based and empirical models to examine the effect of measured microtopographic complexity on ecosystem fluxes. For the first objective, our two main focuses were: i) using a case-study approach, assess how much

114 area needs to be sampled at a given site in order to be able to adequately quantify
115 microtopographic variability within an unpatterned peatland; and ii) using hummock-
116 hollow plots across multiple peatlands, quantify morphometric properties (*e.g.*
117 microtopography height distribution, slope, and roughness) derived from high-resolution
118 surface DEMs, which may be useful as microtopographic metrics.
119

120 **METHODS**

121 ***Experimental design***

122 We first evaluated how much sampling area is needed to capture the overall
123 microtopographic variation of an unpatterned site using both structure-from-motion (SfM)
124 (see Brown and Lowe 2005; Mercer and Westbrook 2016) and a transect-based sampling
125 approach (Figure S1 – middle panel). To accomplish this, we randomly sampled 50 plots
126 for SfM reconstruction in a peatland near Red Earth Creek, AB (56.54°N 115.22°W)
127 (hereafter referred to as site-level). In addition, we manually measured surface elevation
128 along several 50 m transects at 0.05 m intervals covering the plot area at the Red Earth
129 Creek site. Secondly, we used SfM to examine morphometric properties at the plot scale
130 in 9 boreal/hemi-boreal, non-permafrost peatlands (4 in Canada, 4 in USA, 1 in Sweden;
131 see Table 1 and Figure S1 – top panel) using two different approaches. The first approach
132 involved randomly selecting 9 plot locations within a single site and creating a plot around
133 the random location which was perceived to contain a hummock-hollow pair. The second
134 approach involved qualitatively choosing what was perceived to be a representative
135 hummock-hollow pair at 9 different sites. The aim of our approach was to highlight the
136 potential breadth of variation in morphometric properties which might be observed either

137 within a site (*i.e.* implications for small sample size) or across sites (*i.e.* highlight potential
138 challenges with site inter-comparisons without supporting information of peatland
139 microtopographic metrics). For both randomly located plots and qualitatively chosen plots,
140 academic peatlands researchers were asked to identify a central point for a hummock
141 and hollow subplot within the larger microtopography plot.

142 ***Site preparation and image acquisition protocol***

143 All vascular vegetation was removed from the plot area using scissors and hand pruners
144 in order to provide an unobstructed view of the surface microtopographic variation (moss
145 surface) for imaging. Matte-colored discs (n=20) of 0.04 m diameter were placed
146 randomly on the clipped surface to provide reference points for better correlation between
147 images. To provide absolute scale and orientation, two boxes of known dimensions (0.1
148 m × 0.1 m × 0.1 m) were placed in each plot and levelled prior to image acquisition.
149 Images of each target area were taken via at least two circuits around the plot, with
150 images taken from two separate vertical viewing angles (see
151 http://www.cs.cmu.edu/~reconstruction/basic_workflow.html for third party description of
152 general workflow). Distance to target area was set so that a large portion of the clipped
153 area was visible in each image. To produce different horizontal viewing angles, images
154 were taken every one or two paces around the perimeter of the plot. This procedure
155 yielded 41 to 282 overlapping images from multiple view-points of the plot areas, which
156 ranged in size from 3.2 to 10.1 m^2 (Table 1). Images were taken during either clear-sky
157 or over-cast conditions near mid-day during the summer to avoid changing lighting
158 conditions and to limit self-shadowing of the surface. Images were captured with digital
159 cameras using automatic exposure settings. Prior to analysis, all images were

downscaled where necessary to a common resolution of 2048 x 1536 pixels using a Lanczos3 filter.

Digital elevation models of microtopography

A point-cloud of the moss surface was generated using an SfM approach (Brown and Lowe 2005; Mercer and Westbrook 2016) using the program Visual SfM (Wu, 2011). Visual SfM identifies image features for cross-comparison using a scale-invariant feature transform (Lowe, 1999), and then matches features between images in a pairwise manner. Effectively, this creates multiple stereo-pairs from which camera position and scene geometry can be estimated through triangulation. This procedure yielded average point cloud densities ranging from 3-59 pixels cm^{-2} for the imaged plots (Table 1).

Prior to generating the DEMs, point clouds were cropped to the region of interest (*i.e.* area of clipped vegetation), then scaled, levelled, and oriented using the rendered reference objects. DEMs were produced using the MATLAB function *TriScatteredInterp* (MATLAB R2010a, The Mathworks), which performs Delaunay triangulation of the point clouds. DEMs were generated on a 0.01 m x 0.01 m grid using natural neighbor (Voronoi) interpolation. The DEMs were smoothed using a mean filter window with a size of 0.03 m x 0.03 m. Finally, a mask was applied to the DEMs to remove reference objects. The accuracy of the method was assessed (see Appendix 1 and corresponding Figures S2 and S3 in supplemental material) yielding root mean square error values less than 0.01 m in the x, y, z under laboratory conditions. Median absolute deviation of elevation

between the DEM and lab and field validation plots was 0.004 m and 0.018 m, respectively.

Capturing site-level microtopographic variation

Plots from the Red Earth Creek peatland were ~3.5 m^2, and differences between plot elevation for the 50 plots were surveyed using a Smart Leveler digital water level (accuracy ±2.5 mm), with offsets applied to DEMs. A Monte Carlo re-sampling approach was used to evaluate how total variance in microtopographic elevation increased with increasing sample size. For each sample size (*i.e.* 1-50), 200 random re-samplings were performed. To estimate the change in variance with increasing sample size, a rectangular hyperbola was fit to the mean variance (y) versus sample size (x):

$$y = \frac{ax+b-\sqrt{(ax+b)^2-4axbc}}{2c} \quad (1)$$

where *b* is the estimated maximum total variance, and *a* and *c* are initial slope and concavity parameters.

To evaluate the dominant scale of microtopographic variation which contributes to total variance, a fast Fourier transform (*fft* function in MATLAB) was used to estimate the power spectral density (PSD) of microtopographic variation along an artificially constructed 300 m long transect (combination of multiple transects). Manual measurements of moss surface elevation were taken every 0.05 m along multiple connected transects at the Red Earth Creek, AB and Nobel, ON site using the Smart Leveler.

Plot-level microtopographic variation

Plot-level microtopographic variation was analyzed using randomly and qualitatively chosen plot locations listed in Table 1. Based on the hummock-hollow conceptual model, our *a priori* assumption was that a hummock-hollow pair would have a bi-modal distribution of surface elevation. Our null hypothesis was that microtopography would follow a bi-modal distribution, so we evaluated DEM height distributions using 1– to 3–member Gaussian mixture models (GMM) to evaluate whether 2-member GMMs would best explain height distributions. GMMs were fit to DEM height distributions using the MATLAB function *gmmdistribution.fit*, which uses an iterative expectation maximization algorithm to determine GMM parameters representing maximum likelihood estimates. The GMM fit function was seeded with initial parameter estimates using *k*–means cluster analysis. The best model was selected based on the minimum Akaike information criteria (AIC).

Surface slope and aspect were evaluated using the computed surface normals for each point and eight connected neighbours of the DEM. The fractal dimension of plots was evaluated using radially averaged PSD derived from an *fft* of elevation data. The Hurst (*H*) exponent (values of 0–1) presented herein is related to fractal dimension as 3-*H*, where the slope of the PSD curve in log space is -2(H+1).

Modelled moss surface insolation and productivity at the plot-level

Potential moss surface insolation was modelled using the formulation presented in Kumar et al. (1997) to account for earth-sun geometry, surface slope and aspect, and diffuse

227 radiation under clear-sky conditions. Total potential insolation was evaluated on an
228 annual basis and normalized relative to total insolation on a flat surface for each plot
229 location.
230
231 For moss net photosynthesis (NP) and capitula water content (*WC*), each plot was
232 classified into three units based on relative elevation which notionally correspond with
233 hollow/lawn, low hummock, high hummock. K-means clustering was used to perform
234 unsupervised classification of microtopographic elevation (Figure S4). A separate
235 parameterization for moss NP and WC was used for each elevation cluster.
236 Parameterizations for hollow/lawn, low hummock, and high hummock were obtained from
237 *Sphagnum* species of the section Cuspidata, Sphagnum, and Acutifolia, respectively
238 (Figure S5). Empirical relations between WC and water table depth (WTD) were derived
239 from Strack and Price (2009) and Rydin (1985), and were modelled as follows:
240 $$WC = p_1 \cdot \ln(p_2 \cdot WTD) + p_3 \quad (2)$$
241 where WC is the ratio of the mass of water to the sample dry weight (g g^{-1}), and $p_{1\text{-}3}$ are
242 fitted parameters. WC was restricted to a range of 1–25 g g^{-1}. A rational function was
243 used to model the relation between moss capitula NP and WC according to the results in
244 Schipperges and Rydin (1998), where:
245 $$NP_{pot} = 100 \cdot \left(\frac{p_4 \cdot WC^2 + p_5 \cdot WC + p_6}{WC^2 + p_7 \cdot WC + p_8}\right) \cdot NP_{max}^{-1} \quad (3)$$
246 where NP_{pot} represents percentage of maximum NP, and $p_{4\text{-}8}$ are fitted parameters.
247 Estimates of 2.7, 5.6, and 6.5 g m^{-2} day^{-1} for NP_{max} were used to represent *Sphagnum*
248 species of section Cuspidata, Sphagnum, and Acutifolia, respectively (Nungesser, 2003).
249

RESULTS

Site-level microtopographic variation

In characterizing microtopographic variability across the Red Earth Creek site (Figure S1 – middle panel), our data shows that variability in surface elevation increases asymptotically with sample size (*i.e.* area sampled) and is well predicted by a rectangular hyperbola (r^2=0.98; p<<0.01) (Figure 1). Based on the asymptote of the fitted rectangular hyperbola (0.147 m), Figure 1 shows that on average an area of 32 m^2 (*i.e.* 9 random plots of ~3.5 m^2 size) contains roughly 95% of the predicted site-scale microtopographic variability. Even though increasing the number of plots by a factor of 5 (*i.e.* ~50 plots) has little effect on the average variance in surface elevation, the range associated with re-sampling is reduced by about half (Figure 1 – shaded area).

While the Red Earth Creek multi-plot DEM data provides the ability to assess the area required to capture site-scale microtopographic variability for a small unpatterned Alberta peatland, it does not directly provide information on what spatial scales contribute most to overall variability. The power spectral density (PSD) of manual elevation transects from both the Red Earth Creek and Nobel sites suggests that most of the microtopographic variation for these two surveyed sites occurs at spatial scales between 1–10 m (Figure 2 – cumulative curves). Both sites have qualitatively similar PSD curves in log-space with a roll-off at spatial scales between 2.4–2.9 m (break point of piecewise regression). Moreover, the PSD of microtopographic variation appears to be well described by a power law (*i.e.* relatively smooth slope in log space despite noise) at small spatial scales

resulting in a Hurst exponent (see Methods for relation to fractal dimension) between 0.14–0.26. For both transects, 95% of total variance is captured at a length scale greater than ~0.6 m.

Plot-level hypsometry and fractal dimension

There is a characteristic difference in the elevation distribution of whole-plots compared to that of the corresponding hummock-hollow subplots for both qualitatively (Figure 3) and randomly (Figure 4) chosen plot locations. The elevation distributions for hummock-hollow subplots tend to have a clear separation of modes (Figures 3-4 B-panels). The degree of separation in modes has a moderately weak correlation (r^2 = 0.31) but significant linear relation (F_{16} = 7.1, p = 0.017) with the interquartile range in elevation of the whole plot. On average, the elevation range absent from the hummock-hollow subplots represents roughly 31% of the microtopographic range of the whole plot. When all hummock-hollow subplots are aggregated across randomly selected plots (*i.e.* Nobel, ON site), the whole elevation distribution is captured (Figure S6). However, there remains a bias towards higher elevations being sampled in the aggregated subplot elevation distribution compared to the aggregated whole plot elevation distribution.

In testing the null hypothesis of bimodally distributed relative surface elevation at the plot scale, we examined the goodness of fit of one-, two-, and three-member GMMs (see Figure S7 for example GMM fits). An assessment of all 18 plots suggests that two- or three-member GMMs tend to provide a better fit to reconstructed elevation distributions compared to a one-member (*i.e.* normal) distribution. Based on AIC values, the one-

296 member GMM was best for only 3 plots, while two- and three-member GMMs were best
297 for 6 and 9 plots, respectively (Table 2). In contrast, when GMMs were fit to hummock-
298 hollow subplot data, the two-member GMM tended to outperform one- and three-member
299 GMMs.
300
301 The mean (μ) and standard deviation of elevation for hummock and hollow subplots were
302 grouped and compared according to plot selection method (*i.e.* random within site versus
303 qualitative between site selection). Since the μ parameter corresponds with relative
304 elevation, we took the difference between the two members (*i.e.* μ_{hum}–μ_{hol}) for comparison
305 purposes. Overall, the qualitatively chosen plots appear to have similar relative hummock
306 heights (μ_{hum}–μ_{hol}) (0.21±0.08 m) compared to the randomly chosen plots. (0.19±0.09 m)
307 ($F_{1,16}$=0.2; p=0.66). Variation in elevation tended to be higher in hummock subplots
308 (0.031±0.012 m) compared to hollow subplots (0.021±0.008 m) (microform; $F_{1,32}$=9.3,
309 p=0.005), where the difference between hummock and hollow subplots was similar when
310 comparing qualitatively and randomly chosen sites (microform × plot type; $F_{1,32}$=0.05;
311 p=0.82).
312
313 Depending on the underlying structure of spatial variability, surface roughness can be
314 highly dependent on the scale of analysis. A two-dimensional power spectral density of
315 elevation provides a means to formally describe the change in roughness with scale
316 (Figure. 5). The power spectral density of elevation was found to be a linear function of
317 length-scale across the 0.05–1 m range in log–log space (r^2_{adj}>0.97) and is the basis for
318 the Hurst exponent (*H*) (see methods for relation to fractal dimension). While the

distribution of *H* for qualitatively chosen plots (0.70±0.18) was higher compared to randomly chosen plots (0.58±0.10) (*i.e.* comparatively less 'complexity' at finer spatial scales), the difference was not significant ($F_{1,16}$ = 3.06; p = 0.10). Similar to the transect-based analysis (see *Site-level microtopographic variation* section), 95% of total variance is captured at a length scale greater than 0.37-0.90 m.

Plot-level slope, aspect and solar insolation

A Weibull distribution provided a good fit to the slopes for the reconstructed DEMs (Figure S8), where the average, maximum, and minimum RMSE were 0.10%, 0.14%, and 0.06%, respectively, based on a relative frequency distribution with 1° bin sizes. When grouped according to qualitatively versus randomly chosen plots (Table 1), the modal slope for whole plots was 18.6±4.5° and 20.0±4.8°, respectively. Similarly, the distribution of standard deviation in slope for qualitatively and randomly chosen plots was 13.1±1.5° and 12.9±2.0°, respectively. Comparing the parameter distributions from the Weibull fit for qualitatively and randomly chosen plots, it was found that there was no significant difference in the mean scale (analogous to mode) and shape (analogous to standard deviation) parameters (scale: p=0.72, $F_{1,16}$=0.13; shape: p=0.24, $F_{1,16}$=1.47).

While modal slope tended to only be slightly higher in the hummock subplots (20.3±6.9°) versus hollow subplots (16.0±5.1°), there was greater distinction in the prevalence of steep slopes (*i.e.* >45°) in hummock subplots (8.7±8.6%) versus hollow subplots (3.4±5.4%) (Figure S9). Comparing slope in the hummock/hollow subplots to the 3-member GMM clusters (high, intermediate, and low elevations – for example see Figure

S4), we see that the subplots tend to be somewhat flatter compared to the rest of the plot, particularly for hollow subplots (Figure S9).

Figure 7 shows how slope and aspect of the Seney WET plot affect potential solar insolation at the moss surface under ideal conditions (i.e. clear-sky, sparse vegetation), where broadly similar results are obtained for all plots (Figure S10). Potential solar insolation is significantly affected by aspect ($F_{7,24984} \geq 543.9$, $p<<0.01$) (e.g. Figure 7a) and its interaction with slope ($F_{7,45606} \geq 3579.4$, $p<<0.01$) (e.g. Figure 7b) across all plots, where on average, south facing slopes receive double the potential solar insolation compared to north facing slopes. Based on measured slope and aspect at randomly and qualitatively chosen plots, median potential solar insolation for a south-facing slope is 14-25% greater compared to a flat surface. Similarly, for a north-facing slope, median potential solar insolation is 21-45% lower (Figure S10).

Plot-level empirical model of moss productivity using high resolution DEMs

Assuming a flat water table at the plot-level, Figure 8 shows how modelled NP_{pot} varies with WTD relative to the average hollow surface. Hollows tend to have a comparatively narrow range of WTD (*i.e.* 0–0.15 m) over which the moss is expected to be highly productive compared to hummocks. Despite using species-dependent NP_{pot}-WC relations, the large differences in water table range over which hummock and hollow NP_{pot} is high is largely driven by the WC-WTD relations (Figure S5). Where moss species have large differences in NP_{max} and different characteristic water retention, NP_{pot} rarely overlaps between microtopographic classes (Figure 8). If we ignore the effect of species-

365 dependent characteristics (i.e. NP_{max}, NP_{pot}–WC, and WC–WTD) and use a single
366 parameterization (herein low-hummock), differences between microtopographic classes
367 tend to be smaller for shallow water table conditions (Figure S11), yet there remains a
368 characteristic difference in mean NP_{pot} between microtopographic classes.
369
370 From a scaling perspective, modelled NP_{pot} (Figures 8 and S11) was used to compare
371 spatially explicit estimates with averages based on the notional chamber subplot (i.e. pre-
372 determined 0.37 m^2 area in perceived hummock and hollow — see methods and Figure
373 S1, lower panel). In general, spatially explicit NP_{pot} estimates tended to be higher/lower
374 than the scaled hummock-hollow subplot estimates depending on whether the water table
375 was relatively shallow/deep (Figure 9a). The maximum positive bias between the spatially
376 explicit and scaled hummock–hollow subplot NP_{pot} values ranged from 0.52–1.37 g m^{-2}
377 day^{-1} under shallow water table conditions, while the negative bias ranged from -0.22 to
378 -1.98 g m^{-2} day^{-1} under deeper water table conditions. Using a single parameterization for
379 NP_{pot} tends to result more consistently in positive bias between the spatially explicit and
380 scaled hummock-hollow subplot models (Figure 9b), where maximum bias is up to 1.98
381 g m^{-2} day^{-1}. Averaged across all 18 plots, the location of the subjective hummock subplot
382 broadly overlapped with the k-means high-hummock classification (94%), with only small
383 portions overlapping with the low-hummock classification (6%). Similarly, the location of
384 the subjective hollow subplot broadly overlapped with the k-means hollow/lawn
385 classification (79%), with only small portions overlapping with the low-hummock
386 classification (20%). In this study, our results indicate that the subjective choice of
387 hummock and hollow subplot location (e.g. for chamber flux measurement) systematically

388 under-samples intermediate topographic positions. For the NP_{pot} model using separate
389 parameterization for the microtopography classes, the low-hummock class tends to
390 remain distinct from both the hollow/lawn and high-hummock class except under very dry
391 conditions (see Figure S8 for an example). For the uniform parameterization, the low-
392 hummock classification is distinct from the other two classes only under wet conditions.
393 In contrast, the low-hummock classification behaves like the hollow/lawn under
394 moderately dry conditions, and behaves like a high-hummock under very dry conditions.
395
396 Evaluated over a large range of WTD (*i.e.* 0–0.6 m below average hollow surface), the
397 root mean square difference (RMSD) between NP_{pot} (as % of maximum) calculated using
398 the SfM-derived DEMs and binary classification using the average hummock and hollow
399 subplot elevation was 20±6%. However, bias between the DEM-based NP_{pot} and
400 subjective hummock/hollow elevations is greatly reduced if an unbiased binary
401 classification is used. The RMSD when hummock and hollow elevations are set to the
402 66^{th} and 33^{rd} percentile of measured elevation distribution is reduced 5±2% (Figure 10).
403 Moreover, bias is largely eliminated with the use of only several elevation classes where,
404 for example, an RMSD of 1% or less is achieved using 2-7 elevation classes.
405
406
407 **DISCUSSION**
408 ***Assessing microform representativeness***
409 In studies which use the hummock-hollow microtopography classification as part of their
410 sampling design, there are many cases in which the plot choice is said to be

411 representative (*e.g.* Kettridge and Baird 2008; Laing et al., 2008; Nijp et al., 2014), but
412 often lacks detail on how representativeness was assessed. For example, when
413 characterizing the surface within an eddy covariance flux measurement footprint, it is
414 common to only sample one or few hummock-hollow pair(s) (*e.g.* Lafleur et al., 2003;
415 Humphreys et al., 2006; Peichl et al., 2014; Moore et al., 2015). Similarly, for direct
416 measurements of surface fluxes where microtopography is considered explicitly,
417 chamber-based measurements typically use between four and eight replicates (*e.g.*
418 Frenzel and Karofeld 2000; Turetsky et al., 2002; Forbrich et al., 2011; Petrone et al.,
419 2011) per microtopographic unit. For peatland studies which use random plots, as many
420 as 30 plots per site have been reported (*i.e.* Wieder et al., 2009), yet earlier studies have
421 reported using as few as one to four plots to characterize a site (*e.g.* Crill et al., 1988;
422 Shannon and White 1994; Regina et al., 1996). Using the Red Earth Creek results as a
423 reference, for studies which have 4-8 replicates, 2-3 microtopographic units (*e.g.*
424 hummock, lawn, hollow), and the more common chamber size of roughly 0.6 m x 0.6 m,
425 we would infer from our results that the typical total sample area for chamber flux
426 measurements in a peatland ecosystem would capture on the order of 70-86% of site-
427 scale microtopographic variability in their plots. It should be noted however that the simple
428 assessment above assumes that chamber placement is random. In cases with lower
429 replication of two microtopographic units, our results suggest that the uncertainty
430 associated with repeated sampling is relatively high (Figure 1 – shaded area) and that the
431 choice of two microtopographic units could lead to an under-sampling of intermediate
432 topographic positions (*e.g.* Figures 3-4 B-panels). When the ecosystem processes of
433 interest are not measured across the range of variability observed at the site-scale,

particularly for non-linear processes, then scaling from process-based, or simply plot-scale measurements, is at risk of being biased. Our simple empirical model of moss NP_{pot} demonstrates that flux bias can be large relative to NP_{max} and is strongly dependent on water table depth (Figure 9). While water table is a first order control on peat water content (Hayward and Clymo, 1982), moss capitula water content, however, has been shown to be less sensitive to water table (Strack and Price, 2009). Moreover, the sensitivity of *Sphagnum* CO_2 assimilation to water level has been shown to be strongly dependent on precipitation (Robroek et al., 2008). Using the simple empirical model and measured WTD at the Seney site (see Moore et al., 2015), the magnitude of modelled NP_{pot} (seasonal average of 1.2–3.8 g m^{-2} day^{-1}) is less than seasonal average chamber-measured GPP values (see Ballantyne et al., 2014), though the later includes vascular vegetation. Nevertheless, the empirical NP-modelled values are broadly consistent with field measured *Sphagnum* production (e.g. Moore, 1988; Waddington et al., 2003). Although NP_{pot} estimates are strongly influenced by the parameterization used (*e.g.* Figure 8 and S11), there remains a large bias between the spatially explicit and scaled hummock-hollow subplot NP_{pot} models.

To upscale models or plot-scale measurements it is important to determine the microtopographic structure and variability of a peatland. There were often non-bimodal distributions of microtopography in our study sites (Figures 3–4 A-panels and Table 2) where the more continuous distribution of elevation at the plot scale suggests that when experimental designs use hummock-hollow pairs as the primary experimental unit (Figures 3–4 B-panels) they have a tendency to capture the ends of the distribution,

457 omitting on average 25% of the elevation distribution at the plot scale (see also Figure
458 S6). In this study, we clipped vegetation in 50 small random plots to produce very high
459 resolution DEMs for assessing microtope-scale (*i.e.* S3 hummock-hollow complex, *cf*.
460 Belyea and Baird, 2006) variability, yet surface vegetation removal will generally be
461 undesirable. Ground- or drone-based SfM approaches have been used to produce a
462 digital surface model (DSM – vegetation present) for alpine (Mercer and Westbrook,
463 2016) and blanket (Harris and Baird, 2018) peatlands with reasonable accuracy (*e.g.*
464 mean absolute error of ~0.08 m, and normalized median absolute deviation of ~0.11 m
465 for the alpine and blanket peatlands, respectively). In situations where surface vegetation
466 removal is not possible or desirable and/or where drone-based imagery is hampered (*e.g.*
467 treed peatlands), a survey of height distribution along one or several transects would
468 provide an alternative to assessing microtope to mesotope-scale (S3–S4 Belyea and
469 Baird, 2006) microtopographic variability. The power spectral density of transect data
470 would suggest that, for absolute height, a sampling interval of less than 1 m (*e.g.* 0.5 m)
471 would capture the scales of variability which contribute most to total height variance
472 (Figures 2 and 5) since this corresponds to ~95% of measured microtopographic variation
473 and provide sufficient fine-scale data to estimate the fractal dimension of
474 microtopography. Information on height distributions could provide the basis for plot
475 selection, where plots could be chosen to deliberately span the range of variability, or to
476 avoid oversampling extremes. Information on the height distribution would furthermore
477 provide the ability to scale up findings from the plot level given their relative position in
478 the wider distribution of microtopographic variability (*cf. Griffis* et al., 2000).
479

Despite the variety of site characteristics observed, our plots were limited to bogs and poor fens, and did not include sites with ridge and pool patterning. Nevertheless, our results would suggest that generalizations based on a hummock-hollow classification, either to the site-scale, or to hummocks-hollow pairs across sites should be viewed with a degree of skepticism when sample size is low, or when a general microtopographic survey is absent/unreported. Thus, for wider inter-comparability of peatland studies, SfM or transect-based approaches of measuring and reporting on one or several morphometric properties of microtopography could provide a more comprehensive dataset to aid in future meta-analysis/synthesis.

Implications for appropriate complexity ecosystem modelling in peatlands

The complex shape/structure of peatland microtopography has generally been ignored from a modelling standpoint, but several studies have shown, for example, that slope and aspect may affect peat temperature (Kettridge and Baird 2010). Under clear-sky conditions, modelled annual total solar insolation differs from a flat surface by roughly ±20% in our measured plots, where our study sites span 43° to 60°N latitude (Figure S10). For north and south facing slopes, this effect is amplified (Figure 7) particularly for high- and low-hummock microtopographic classes (*e.g.* Figure S4), which tend to have greater average slope compared to the hollow/lawn classification (Figure S9). While our study sites are limited to the non-permafrost boreal region, the applicability of slope and aspect considerations to modelling tundra tussocks in arctic and permafrost regions is also relevant (*e.g.* De Baets et al., 2016). Based on the results of empirical studies, the shape of microtopographic features ought to play a role in ecosystem fluxes due to the effect of

503 shortwave radiation on surface evaporation (Kettridge and Baird, 2010),
504 photosynthetically active radiation on moss production (Harley et al., 1989; Loisel et al.,
505 2012), and soil temperature on methane production and respiration (*e.g.* Lafleur et al.,
506 2005; Waddington et al., 2009). It is important to note, however, that under cloudy
507 conditions the increasing proportion of total insolation from diffuse radiation decreases
508 the disparity in insolation associated with slope and aspect. Furthermore, in peatlands
509 where substantial tree, shrub, or graminoid cover exists, the importance of slope and
510 aspect on soil heating or ecosystem fluxes is likely to be low since insolation decreases
511 exponentially with increasing vascular leaf area.
512
513 In addition to microtopographic shape/structure, the size of microtopographic features
514 and their small-scale variability can similarly affect ecosystem fluxes, where height above
515 water table imposes a first order control on water availability. Methane fluxes from
516 peatlands, for example, have been shown to vary logarithmically over 0.1 m scales
517 (Turetsky et al., 2014). Water availability at the moss surface has been shown to be both
518 species-dependent and strongly affected by water table (Hayward and Clymo, 1982;
519 Rydin, 1985), where moss species and water availability has been linked to many
520 ecohydrological processes such as surface evaporation (Kettridge and Waddington,
521 2014), productivity (Williams and Flanagan, 1998; Strack and Price, 2009), and
522 hydrophobicity (Moore et al., 2017). We show that when microtopographic variability is
523 explicitly modelled, complex patterns of potential moss productivity emerge (Figure S12)
524 which are not necessarily captured by a hummock-hollow model (Figure 9), and that the
525 presence of bias is independent of whether moss species niche partitioning is considered.

The SfM method is a potentially useful tool for examining how morphometric properties of the surface which affect ecohydrological processes vary within a site. Moreover, information on microtopographic variability from SfM-derived DEMs can be used to further examine the potential role of fine-scale microtopographic variability on biogeochemical processes within a modelling domain. The GMM is a simple way to include a more realistic description of height distributions within distributed peatland models (*e.g*. Dimitrov et al., 2010), or extend from the meso- to micro-scale (Sonnentag et al., 2008). Computationally, GMMs are a relatively efficient way of representing microtopographic variability, needing only two parameters per member of the GMM distribution. Conceptually, the GMM distribution can be applied directly in distributed peatland models to populate relative heights of individual cells. In the case of one-dimensional models, a GMM distribution can be used as a transfer function for any water table-dependent processes, particularly in cases where the relation is non-linear. Alternatively, a small number of parameters from the PSD of microtopographic elevation (*e.g.* variance, Hurst exponent, and spatial scale of break point), be it from a transect (Figure 2) or DEM (Figure 5), can be used to generate 'synthetic' microtopography which includes spatial structure in elevation change rather than just the distribution.

CONCLUSIONS

The magnitude of variation in assessed morphometric properties within a site (randomly chosen plots) is commensurate with the range across sites (qualitative plots), where mean differences are comparatively small. With a small effect size, our results highlight

549 the need for adequate spatial sampling in process-based studies of microform function,
550 particularly when upscaling to the whole peatland or in order to make broader inferences
551 regarding peatland microforms in general. The SfM technique provides very high
552 resolution and accurate DEMs relatively quickly and easily. For studies which focus on
553 processes which are correlated with microtopographic position, a DEM or DSM derived
554 from ground- or drone-based imagery provides valuable information on microtopographic
555 variability and structure which can help inform plot selection, be used for upscaling
556 results, and quantify well defined morphometric and topographic variables to aid in study
557 inter-comparisons. Conversely, height measurements (*e.g.* using a dGPS or other survey
558 method) along a transect of at least 100 m with measurements taken at an interval of less
559 than 1 m provides sufficient information to describe a number of peatland morphometric
560 properties (*e.g.* hypsometry, roughness, fractal dimension, etc.).

561

562 Our study highlights the need to critically assess sampling approaches in peatland
563 ecosystem science, where we show that a strict hummock-hollow classification tends to
564 under-sample intermediate topographic positions. While the discretization of peatland
565 ecosystems into microtopographic units has facilitated the understanding of peatland
566 processes in the context of species niche partitioning and their covariates such as water
567 table position, we now have techniques to better quantify variability with relative ease.
568 Consequently, techniques such as SfM enable us to consider peatland ecosystem
569 processes as part of a continuum. We must recognize that our conceptualizations, while
570 perhaps representing necessary simplifications, ought to be scrutinized to ensure that
571 elements of peatland complexity are not omitted. By considering microtopography

explicitly, we may be better able to understand how ecosystem complexity subsumed within current microtopographic classifications might represent an important unquantified confounding variable which limits our ability to adequately resolve and thus understand certain peatland processes.

CODE/DATA AVAILABILITY

All data necessary to reproduce the results in the paper are available via 10.5281/zenodo.2545674. The data set also includes the script used to carry out all final analysis and figure production. Raw imagery or point clouds can be obtained by contacting the corresponding author directly.

AUTHOR CONTRIBUTIONS

PAM, JMW, DKT, NK, and GG designed the study. All co-authors contributed to in-situ data collection. Data post-processing and analysis was primarily done by PAM. PAM prepared the manuscript, with substantive editing and comments from all other co-authors.

COMPETING INTERESTS

The authors declare that they have no conflict of interest.

ACKNOWLEDGEMENTS

We would like to thank James Sherwood and Paul Morris for valuable conversations regarding the feasibility of this study and early discussions regarding research design. We thank Lorna Harris for comments on an earlier draft of this manuscript. We also thank Tom Ulanowski for data collection for the James Bay site, Rebekah Ingram and Kristyn Mayner for data collection at the Red Earth Creek site, Mandy MacDougall, Alanna Smolarz and Alex Furukawa for assistance with the Nobel data collection and analysis, and to Lee Slater for data collection in Maine. Finally, we would like to thank Dr. Kutzbach and an anonymous reviewer for valuable comments and suggestions which helped to improve the manuscript. This research was supported by a NSERC Discovery Grant and NSERC Discovery Accelerator Supplement to JMW.

REFERENCES

Andrus, R., Wagner, D., and Titus, J.: Vertical zonation of *Sphagnum* mosses along hummock-hollow gradients, Can. J. Bot., 61, 3128-3139, doi:10.1139/b83-352, 1983.

Belyea, L. R., and Baird, A. J.: Beyond "the limits to peat bog growth'": Cross-scale feedback in peatland development, Ecol.l Monogr., 76, 299–322, doi: 10.1890/0012-9615(2006)076[0299:BTLTPB]2.0.CO;2,2006.

Belyea, L. R., and Clymo, R. S.: Do hollows control the rate of peat bog growth. *Patterned mires and mire pools*, 55-65, 1998.

Belyea, L. R., and Clymo, R. S.: Feedback control of the rate of peat formation. Proc. of the Royal Soc. London B: Biol. Sci., 268, 1315-1321, doi:10.1098/rspb.2001.1665, 2001.

Belyea, L. R., and Malmer, N.: Carbon sequestration in peatland: Patterns and mechanisms of response to climate change, Glob. Chang. Biol. 10, 1043–1052, doi.org/10.1111/j.1529-8817.2003.00783.x, 2004.

Benscoter, B. W., Wieder, R. K., and Vitt, D. H.: Linking microtopography with post-fire succession in bogs, J. Veg. Sci., 16, 453–460, doi:10.1111/j.1654-1103.2005.tb02385.x, 2005.

Blodau, C., Basiliko, N., and Moore, T. R.: Carbon turnover in peatland mesocosms exposed to different water table levels, Biogeochem., 67, 331-351, doi:10.1023/B:BIOG.0000015788.30164.e2, 2004.

Brown, M., and Lowe, D. G.: Unsupervised 3D object recognition and reconstruction in

unordered datasets. Fifth International Conference on 3-D Digital Imaging and Modeling, 56-63, doi:10.1109/3DIM.2005.81, 2005.

Bruland, G. L, and Richardson, C. J.: Hydrologic, edaphic, and vegetative responses to microtopographic reestablishment in a restored wetland, Rest. Ecol., 13, 515-523, doi:10.1111/j.1526-100X.2005.00064.x, 2005.

Bubier, J. L., Moore, T. R., and Roulet, N. T.: Methane emissions from wetlands in the midboreal region of Northern Ontario, Canada, Ecol., 74, 2240-2254, doi: 10.2307/1939577, 1993.

Campbell, D. R., Duthie, H. C., and Warner, B. G.: Post-glacial development of a kettle-hole peatland in southern Ontario, Ecosci., 4, 404-418, doi:10.1080/11956860.1997.11682419, 1997.

Cresto Aleina F., Runkle B. R. K., Kleinen T., Kutzbach L., Schneider J., Brovkin V.: Modeling micro-topographic controls on boreal peatland hydrology and methane fluxes, Biogeosci., 12, 5689-5704, doi: 10.5194/bg-12-5689-2015, 2015.

Crill, P. M., Bartlett, K. B., Harriss, R. C., Gorham, E., Verry, E. S., Sebacher, D. I., Madzar, L., and Sanner, W.: Methane flux from Minnesota peatlands, Global Biogeochem. Cycles, 2, 371-384, doi:10.1029/GB002i004p00371, 1988.

De Baets, S., van de Weg, M. J., Lewis, R., Steinberg, N., Meersmans, J., Quine, T. A., Shaver, G. R., and Hartley, I. P.: Investigating the controls on soil organic matter decomposition in tussock tundra soil and permafrost after fire, Soil Biol. Biochem., 99, 108-116, doi: 10.1016/j.soilbio.2016.04.020, 2016.

Dimitrov, D. D., Grant, R. F., Lafleur, P. M., and Humphreys, E. R.: Modeling peat thermal regime of an ombrotrophic peatland with hummock–hollow microtopography, Soil Sci. Soc. Am. J., 74, 1406-1425, doi:10.2136/sssaj2009.0288, 2010.

Eppinga, M., Rietkerk, M., Borren, W., Lapshina, E. D., Bleuten, W., and Wassen, M. J.: Regular surface patterning of peatlands: Confronting theory with field data, *Ecosystems*, 11, 520–536, doi:10.1007/s10021-008-9138-z, 2008.

Forbrich, I., Kutzbach, L., Wille, C., Becker, T., Wu, J., and Wilmking, M.: Cross-evaluation of measurements of peatland methane emissions on microform and ecosystem scale using high-resolution landcover classification and source weight modelling, Ag. For. Met., 151, 864-874, doi:10.1016/j.agrformet.2011.02.006, 2011.

Frenzel. P, and Karofeld, E.: CH_4 emission from a hollow-ridge complex in a raised bog: The role of CH_4 production and oxidation, Biogeochem., 51, 91-112, doi:10.1023/A:1006351118347, 2000.

Granath, G., Wiedermann, M. M., and Strengbom, J.: Physiological responses to nitrogen and sulphur addition and raised temperature in *Sphagnum balticum*, Oecologia, 161, 481-490, doi:10.1007/s00442-009-1406-x, 2009.

Griffis, T. J., Rouse, W. R., and Waddington, J. M.: Scaling net ecosystem exchange from the community to the landscape level at a subarctic fen, Glob. Change Biol., 6, 459-473, doi: 10.1046/j.1365-2486.2000.00330.x, 2000.

Harley, P. C., Tenhunen, J. D., Murray, K. J., and Beyers, J.: Irradiance and temperature effects on photosynthesis of tussock tundra Sphagnum mosses from the foothills of

667 the Philip Smith Mountains, Alaska, Oecologia, 79(2), 251-259, doi:
668 10.1007/BF00388485, 1989.

669 Harris, A., and Baird, A. J., Microtopographic Drivers of Vegetation Patterning in Blanket
670 Peatlands Recovering from Erosion, Ecosystems, 1-20, doi: 10.1007/s10021-018-
671 0321-6, 2018.

672 Hayward, P. M., and Clymo, R. S.: Profiles of water content and pore size in Sphagnum
673 and peat, and their relation to peat bog ecology. Proceedings of the Royal Society of
674 London. Series B. Biological Sciences, 215(1200), 299-325, 1982.

675 Hodgkins, S. B., Richardson, C. J., Dommain, R., Wang, H., Glaser, P. H., Verbeke, B.,
676 Winkler, R. B., Cobb, A. R., Rich, V. I., Missilmani, M., Flanagan, N., Ho, M., Hoyt, A.
677 M., Harvey, C. F., Vining, S. R., Hough, M. A., Moore, T. R., Richard, P. J. H., De La
678 Cruz, F. B., Toufaily, J., Hamdan, R., Cooper, W. T., and Chanton, J. P.: Tropical
679 peatland carbon storage linked to global latitudinal trends in peat recalcitrance. Nature
680 Comm., 9, 3640, doi: 10.1038/s41467-018-06050-2, 2018.

681 Humphreys, E. R., Lafleur, P. M., Flanagan, L. B., Hedstrom, N., Syed, K. H., Glenn, A.
682 J., and Granger, R.: Summer carbon dioxide and water vapor fluxes across a range of
683 northern peatlands, J. Geophys. Res., 111, G04011, doi:10.1029/2005JG000111,
684 2006.

685 Ise, T., Dunn, A. L., Wofsy, S. C., and Moorcroft, P. R.: High sensitivity of peat
686 decomposition to climate change through water-table feedback, Nature Geosci., 1,
687 763-766, doi:10.1038/ngeo331, 2008.

688 Kettridge, N., and Baird, A. J.: Modelling soil temperatures in northern peatlands, Eur. J.
689 Soil Sci., 59, 327–338, doi:2389.2007.01000.x, 2008.

690 Kettridge, N., and Baird, A.: Simulating the thermal behavior of northern peatlands with a
691 3‐D microtopography, J. Geophys. Res.: Biogeosciences, 115, G03009, doi:
692 10.1029/2009JG001068, 2010.

693 Kettridge, N., and Waddington, J.M.: Towards quantifying the negative feedback
694 regulation of peatland evaporation to drought, Hydrological Processes, 28(11), 3728-
695 3740, doi: 10.1002/hyp.9898, 2014.

696 Kettridge, N., Comas, X., Baird, A., Slater, L., Strack, M., Thompson, D., Jol, H., and
697 Binley, A.: Ecohydrologically important subsurface structures in peatlands revealed by
698 ground-penetrating radar and complex conductivity surveys, J. Geophys. Res., 113,
699 G04030, doi:10.1029/2008JG000787, 2008.

700 Kettridge, N., Turetsky, M. R., Sherwood, J. H., Thompson, D. K., Miller, C. A., Benscoter,
701 B. W., and Waddington, J. M.: Moderate drop in water table increases peatland
702 vulnerability to post-fire regime shift, Sci. Rep., 5, 8063, doi:10.1038/srep08063, 2015.

703 Kumar, L., Skidmore, A. K. and Knowles, E.: Modelling topographic variation in solar
704 radiation in a GIS environment. International Journal of Geographical Information
705 Science, 11(5), 475-497, doi: 10.1080/136588197242266, 1997.

706 Lafleur, P. M., Roulet, N. T., Bubier, J. L., Frolking, S., and Moore, T. R.: Interannual
707 variability in the peatland-atmosphere carbon dioxide exchange at an ombrotrophic
708 bog. Glob. Biogeochem. Cycles, 17, 1036, doi:10.1029/2002GB001983, 2003.

709 Lafleur, P. M., Moore, T. R., Roulet, N. T., and Frolking, S.: Ecosystem respiration in a
710 cool temperate bog depends on peat temperature but not water table, Ecosystems, 8,
711 619-629, doi:10.1007/s10021-003-0131-2, 2005.

712 Laing, C. G., Shreeve, T. G., and Pearce, D. M. E.: Methane bubbles in surface peat
713 cores: in situ measurements, Glob. Change Biol., 14, 916–924, doi:10.1111/j.1365-
714 2486.2007.01534, 2008.

715 Larsen, L. G., Eppinga, M. B., Passalacqua, P., Getz, W. M., Rose, K. M. and Liang, M.:
716 Appropriate complexity landscape modeling, Earth Sci. Rev., 160, 111-130,
717 doi:10.1029/2008JG000787, 2016.

718 Loisel, J., Gallego-Sala, A. V., and Yu, Z. C.: Global-scale pattern of peatland Sphagnum
719 growth driven by photosynthetically active radiation and growing season length,
720 Biogeosciences, 9, 2737-2746, doi: 10.5194/bg-9-2737-2012, 2012.

721 Lowe, D. G.: Object recognition from local scale-invariant features. The proceedings of
722 the seventh IEEE international conference on Computer vision, 2, 1150-1157,
723 doi:10.1109/ICCV.1999.790410, 1999.

724 Lukenbach, M. C., Kettridge, N., Devito, K. J., Petrone, R. M., and Waddington, J. M.:
725 Hydrogeological controls on post-fire moss recovery in peatlands, J. Hydrol., 530, 405-
726 418, doi:10.1016/j.jhydrol.2015.09.075, 2015.

727 Maholtra, A., Roulet, N. T., Wilson, P., Giroux-Bougard, X., and Harris, L. I.:
728 Ecohydrological feedbacks in peatlands: an empirical test of the relationship among
729 vegetation, microtopography and water table, Ecohydrol., 9, 1346-1357,

730 doi:1002/eco.1731, 2016.

731 MathWorks, Inc.: MATLAB, Version 8.5, MathWorks, Natick, Mass., 2015.

732 Mercer, J. J., and Westbrook, C. J.: Ultrahigh-resolution mapping of peatland microform
733 using ground-based structure from motion with multiview stereo, J. Geophys. Res.
734 Biogeosci., 121, 2901-2916, doi:10.1002/2016JG003478, 2016.

735 Moore, T. R.: Growth and net production of Sphagnum at five fen sites, subarctic eastern
736 Canada. Canadian Journal of Botany, 67(4), 1203-1207, doi: 10.1139/b89-156, 1989.

737 Moore, T. R., and Roulet, N. T., and Waddington, J. M.: Uncertainty in predicting the effect
738 of climatic change on the carbon cycling of Canadian peatlands, Clim. Change, 40,
739 229-245, doi:10.1023/A:1005408719297, 1998.

740 Moore, P. A., Morris, P. J., and Waddington, J. M.: Multi-decadal water table manipulation
741 alters peatland hydraulic structure and moisture retention, Hydrol. Proc., 29, 2970-
742 2982, doi:10.1002/hyp.10416, 2015.

743 Moore, P. A., Lukenbach, M. C., Kettridge, N., Petrone, R. M., Devito, K. J. and
744 Waddington, J. M.: Peatland water repellency: Importance of soil water content, moss
745 species, and burn severity, Journal of Hydrology, 554, 656-665, doi:
746 10.1016/j.jhydrol.2017.09.036, 2017.

747 Moore, P. A., Smolarz, A. G., Markle, C. E., and Waddington, J. M.: Hydrological and
748 thermal properties of moss and lichen species on rock barrens: Implications for turtle
749 nesting habitat, Ecohydrol., 12, e2057, doi:10.1002/eco.2057, 2019.

750 Moser, K., Ahn, C., and Noe, G.: Characterization of microtopography and its influence
751 on vegetation patterns in created wetlands, Wetlands, 27, 1081-1097, doi:
752 10.1672/0277-5212(2007)27[1081:COMAII]2.0.CO;2, 2007.

753 Nijp, J. J., Limpens, J., Sjoerd, K. M., van der Zee, E. A. T. M., Berendse, F., and Robroek,
754 B. J. M.: Can frequent precipitation moderate the impact of drought on peatmoss
755 carbon uptake in northern peatlands? New Phytol., 203, 70-80,
756 doi:10.1111/nph.12792, 2014.

757 Nungesser, M. K.: Modelling microtopography in boreal peatlands: hummocks and
758 hollows, Ecol. Mod., 165, 175-207, doi:10.1016/S0304-3800(03)00067-X, 2003.

759 Pedrotti, E., Rydin, H., Ingmar, T., Hytteborn, H., Turunen, P., and Granath, G.:
760 Fine-scale dynamics and community stability in boreal peatlands: revisiting a fen
761 and a bog in Sweden after 50 years, Ecosphere, 5, 133, doi: 10.1890/ES14-
762 00202.1, 2014.

763 Peichl, M., Öquist, M., Löfvenius, M.O., Ilstedt, U., Sagerfors, J., Grelle, A., Lindroth, A.,
764 and Nilsson, M.B.: A 12-year record reveals pre-growing season temperature and
765 water table level threshold effects on the net carbon dioxide exchange in a boreal fen,
766 Env. Res. Lett., 9, 055006, doi: 10.1088/1748-9326/9/5/055006, 2014.

767 Pelletier, L., Garneau, M., and Moore, T. R.: Variation in CO_2 exchange over three
768 summers at microform scale in a boreal bog, Eastmain region, Québec, Canada, J.
769 Geophys. Res., 116, G03019, doi:10.1029/2011JG001657, 2011.

770 Petrone, R. M., Solondz, D. S., Macrae, M. L., Gignac, D., and Devito, K. J.:

771 Microtopographical and canopy cover controls on moss carbon dioxide exchange in a
772 western Boreal Plain peatland. Ecohydrol., 4, 115-129, doi:10.1002/eco.139, 2011.

773 Rahman, M. M., McDermid, G. J., Strack, M., and Lovitt, J.: A new method to map
774 groundwater table in peatlands using unmanned aerial vehicles, Rem. Sens., 9, 1057,
775 doi: 10.3390/rs9101057 , 2017.

776 Regina, K., Nykänen, H., Silvola, J., and Martikainen, P. J.: Fluxes of nitrous oxide from
777 boreal peatlands as affected by peatland type, water table level and nitrification
778 capacity, Biogeochem., 35, 401-418, doi:10.1007/BF02183033, 1996.

779 Robroek, B. J., Schouten, M. G., Limpens, J., Berendse, F. and Poorter, H.: Interactive
780 effects of water table and precipitation on net CO2 assimilation of three co‐occurring
781 Sphagnum mosses differing in distribution above the water table, Global Change
782 Biology, 15(3), 680-691, doi: 10.1111/j.1365-2486.2008.01724.x,2009.

783 Rydin, H.: Effect of water level on desiccation of *Sphagnum* in relation to surrounding
784 Sphagna, Oikos, 45(3), 374-379, doi: 10.2307/3565573, 1985.

785 Rydin, H., and Mcdonald, A. J. S.: Tolerance of *Sphagnum* to water level, J. Bryol., 13,
786 571-578, doi:10.1179/jbr.1985.13.4.571.,1985.

787 Shannon, R. D., and White, J. R.: A three-year study of controls on methane emissions
788 from two Michigan peatlands, Biogeochem., 27, 35-60, doi:10.1007/BF00002570,
789 1994.

790 Sonnentag, O., Chen, J. M., Roulet, R. T., Ju, W., and Govind, A.: Spatially explicit
791 simulation of peatland hydrology and carbon dioxide exchange: Influence of mesoscale

topography, J. Geophys. Res., 113, G02005, doi:10.1029/2007JG000605, 2008.

Strack, M., and Price, J.S.: Moisture controls on carbon dioxide dynamics of peat - *Sphagnum* monoliths. Ecohydrology, 2(1), 34-41, doi: 10.1002/eco.36, 2009

Turetsky, M., Wieder, K., Halsey, L., and Vitt, D.: Current disturbance and the diminishing peatland carbon sink, Geophys. Res. Lett., 29, 1526, doi:10.1029/2001GL014000, 2002.

Turetsky, M. R., Kotowska, A., Bubier, J., Dise, N. B., Crill, P., Hornibrook, E. R. C., Minkkinen, K., Moore, T. R., Myers-Smith, I. H., Nykänen, H., Olefeldt, D., Rinne, J., Saarnio, S., Shurpali, N., Tuittila, E-S., Waddington, J. M., White, J. R., Wickland, K. P., and Wilmking, M.: A synthesis of methane emissions from 71 northern, temperate, and subtropical wetlands, Glob. Change Biol., 20, 2183-2197, doi:10.1111/gcb.12580, 2014.

Ulanowski, T. A., and Branfireun, B. A.: Small-scale variability in peatland pore-water biogeochemistry, Hudson Bay Lowland, Canada, Sci. Tot, Environ., 454-455, 211-218, doi:10.1016/j.scitotenv.2013.02.087, 2013.

Waddington, J. M., and Roulet, N. T.: Atmosphere-wetland carbon exchanges: Scale dependency of CO_2 and CH_4 exchange on the developmental topography of a peatland, Global Biogeochem. Cycles, 10, 233-245, doi:10.1029/95GB03871, 1996.

Waddington, J. M., Rochefort, L. and Campeau, S.: Sphagnum production and decomposition in a restored cutover peatland. Wetlands Ecology and Management, 11, 85-95, doi: 10.1023/A:1022009621693, 2003.

Waddington, J. M., Harrison, K., Kellner, E., and Baird, A. J.: Effect of atmospheric pressure and temperature on entrapped gas content in peat, Hydrol. Proc., 23, 2970-2980, doi: 10.1002/hyp.7412, 2009.

Waddington, J. M., Morris, P. J., Kettridge, N., Granath, G., Thompson, D. K., and Moore, P. A.: Hydrological feedbacks in northern peatlands, Ecohydrology, 8, 113-127, doi:10.1002/eco.1493, 2015.

Wieder, R. K., Scott, K. D., Kamminga, K, Vile, M. A., Vitt, D. H., Bone, T., Xu, B. I., Benscoter, B. W., and Bhatti, J. S.: Postfire carbon balance in boreal bogs of Alberta, Canada, Glob. Change Biol., 15, 63-81, doi:10.1111/j.1365-2486.2008.01756.x, 2009.

Williams, T. G., and Flanagan, L. B.: Measuring and modelling environmental influences on photosynthetic gas exchange in Sphagnum and Pleurozium. Plant, Cell & Environment, 21(6), 555-564, doi: 10.1046/j.1365-3040.1998.00292.x,1998.

Wu, C.: VisualSFM: A visual structure from motion system, 2011.

Yu, Z. C.: Northern peatland carbon stocks and dynamics: a review, Biogeosci., 9, 4071–4085, doi: 10.5194/bg-9-4071-2012, 2012.

Yu, Z., Beilman, D. W., and Jones, M. C.: Sensitivity of northern peatland carbon dynamics to Holocene climate change, Carbon cycling in northern peatlands, pages 55-69, doi:10.1029/2008GM000822, 2009.

Table 1: Summary information, including latitude (Lat.) and longitude (Lon.), on sample locations and SfM reconstructions of microtopographic variation for randomly and qualitatively chosen plots. Sites listed below correspond only to those for plot-level analyses.

Location	Plot Name	Lat.	Lon.	Plot Area (m^2)	Number of Images Used	Point Cloud Density (m^{-2})
Random						
Nobel, ON[1]	Alpha	45.434	-80.081	4.6	47	6.04×10^4
--	Beta	--	--	3.8	41	7.83×10^4
--	Gamma	--	--	4.1	44	6.68×10^4
--	Epsilon	--	--	5.2	53	8.38×10^4
--	Zeta	--	--	6.12	66	1.60×10^5
--	Eta	--	--	5.74	60	1.42×10^5
--	Iota	--	--	5.66	49	3.23×10^4
--	Kappa	--	--	5.53	66	1.77×10^5
--	Theta	--	--	5.48	59	1.38×10^5
Qualitative						
Caribou Bog, MN[2]	Maine	44.83	-68.75	10.1	79	3.75×10^4
James Bay, ON[3]	JamesBay	52.846	-83.930	7.6	82	1.97×10^5
Ottawa, ON	Limerick	44.877	-75.609	9.0	282	5.94×10^5
Puslinch, ON[4]	Puslinch	43.407	-80.264	6.45	109	1.12×10^5
Rödmossen, SWE[5]	Sweden	60.013	17.355	10.6	105	4.71×10^4
Seney, MI[6]	WET	46.190	-86.019	7.7	135	1.12×10^5
Seney, MI[6]	INT	46.192	-86.019	7.0	109	9.44×10^4
Seney, MI[6]	DRY	46.186	-86.015	7.3	62	8.89×10^4
Nobel, ON[1]	Lambda	45.434	-80.081	8.2	61	1.18×10^4

For detailed site information see the following studies: 1. Moore et al., (2019); 2. Kettridge et al. (2008); 3. Ulanowski and Branfireuen (2013); 4. Campbell et al. (1997); 5. Granath et al. (2009); 6. Moore et al. (2015).

sian mixture model (GMM) fit to elevation d for the GMM which minimizes AIC. Plots respective site.

tion	3rd distribution		
Scale	Mean	SD	Scale
0.36	0.28	0.06	0.41
0.53	0.29	0.04	0.10
0.30	0.31	0.05	0.64
0.59	0.44	0.06	0.18
—	—	—	—
0.18	—	—	—
0.76	—	—	—
0.60	0.42	0.05	0.06
0.16	—	—	—
0.55	0.28	0.07	0.30
—	—	—	—
0.62			
—	—	—	—
0.13	—	—	—
0.25	0.44	0.03	0.16
0.40	0.53	0.02	0.09
0.45	0.34	0.05	0.50
0.54	—	—	—

LIST OF FIGURES:

Figure 1: Site-level relation between standard deviation of microtopographic variation based on total sample area for the Red Earth Creek site based on fifty ~3.5 m^2 plots. The grey shaded area represents the 2.5 and 97.5 percentile of standard deviation from the Monte Carlo resampling procedure.

Figure 2: Site-level absolute (solid lines) and cumulative (dashed lines) power spectral density of height along a 300 m transect for the Red Earth Creek, AB (red) and Nobel, ON (black) sites.

Figure 3: Plot-level relative frequency distribution of height in plots where a perceived representative hummock and adjacent hollow was subjectively chosen for a given site (Table 1 – Qualitative plot locations). Relative height distributions are shown for the entire plot (A) and for a hummock and hollow subplot (B) whose area corresponds to the size of a large flux measurement chamber. Elevations are referenced to the lowest point of the reconstructed surface and set to zero.

Figure 4: Plot-level relative frequency distribution of height in plots with randomly chosen locations within a site containing a perceived hummock and adjacent hollow (Table 1 – Random plot locations). Relative height distributions are shown for the entire plot (A) and for a hummock and hollow subplot (B) whose area corresponds to the size of a large flux measurement chamber. Elevations are referenced to the lowest point of the reconstructed surface and set to zero.

867

868 Figure 5: Plot-level radially averaged power spectral density for randomly– (left panel)
869 and qualitatively– (right panel) chosen plots (Table 1) representing the change in
870 elevation variability with length scale. The slope between the power spectral density and
871 wavelength in log-log space corresponds with the Hurst exponent (*H*), where slope = -
872 2(*H*+1); and is related to the fractal dimension as 3-*H*.

873

874 Figure 6: Plot-level Weibull probability density function of slope derived from the surface
875 normal of a planar fit to elevation in a moving 0.03 m x 0.03 m window for all DEMs.
876 Panels (a) and (b) separate the randomly and qualitatively chosen plots, respectively.

877

878 Figure 7: Variation in potential solar insolation relative to a flat surface based on aspect
879 (a) and slope (b). Boxplots shows median and inter-quartile range, with outliers shown as
880 dots. Insolation as a function of slope has been bin averaged per cardinal direction, where
881 each point represents 100 data points. Slope and aspect data are for the Seney, WET
882 plot.

883

884 Figure 8: Plots-scale mean potential net photosynthesis (NP) for three microtopographic
885 classes (i.e. high-hummock, low-hummock, and lawn/hollow — see supplementary figure
886 1) derived from spatially explicit elevation data for random (a,c) and qualitatively chosen
887 (b,d) plots. NP-WC and WC-WTD relations are based on separate parameterization for
888 each microtopography class (see Figure S5).

889

Figure 9: Difference in plot-scale potential net photosynthesis (NP_{pot}) between models using the measured distribution of elevation over the entire SfM-derived DEM and the measured distribution within hummock-hollow subplots. NP_{pot} is modelled using separate parameterization (see Figure S5) for each microtopography class (a), as well as a uniform (low-hummock) parameterization across microtopography classes (b).

Figure 10: Difference in plot-scale potential net photosynthesis (NP_{pot} – as a percentage of max) based on a coarse to fine discretization of elevation values (n_z = 2 to 30) (see Figure S13 for example). NP_{pot} is modelled using separate parameterizations (see Figure S5) for each microtopography class (a), as well as a uniform (low-hummock) parameterization across microtopography classes (b). RMSE was calculated using NP_{pot} from the original plot-level DEMs as the reference values. Discretized elevation values for each plot are based on elevation percentiles ($p_{z,i}$) where $p_{z,i} = (i-1)\frac{100}{n_z} + \frac{50}{n_z}$; for i=1 to n_z.

906 [Figure 1]

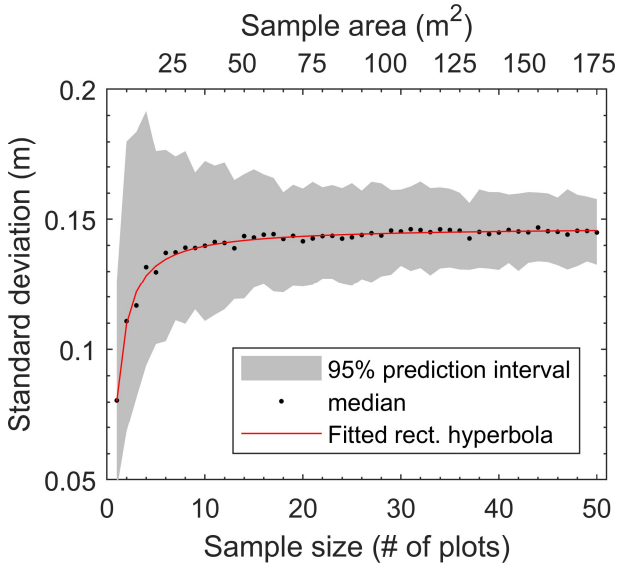

907

908

909 [Figure 2]

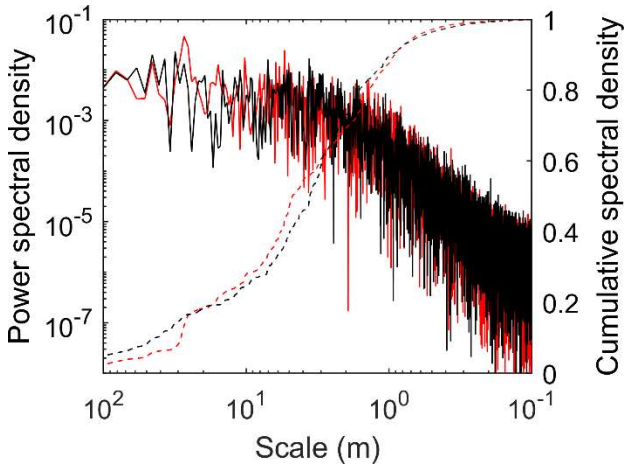

910

911

912 [Figure 3]

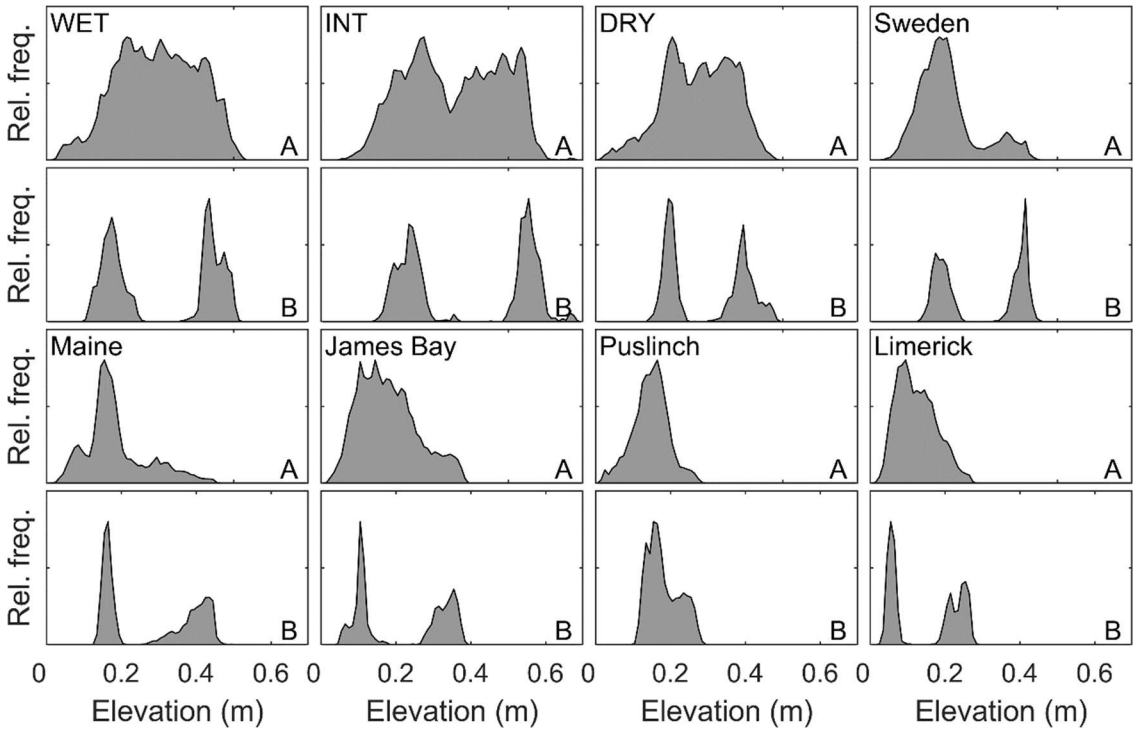

913

914

915 [Figure 4]

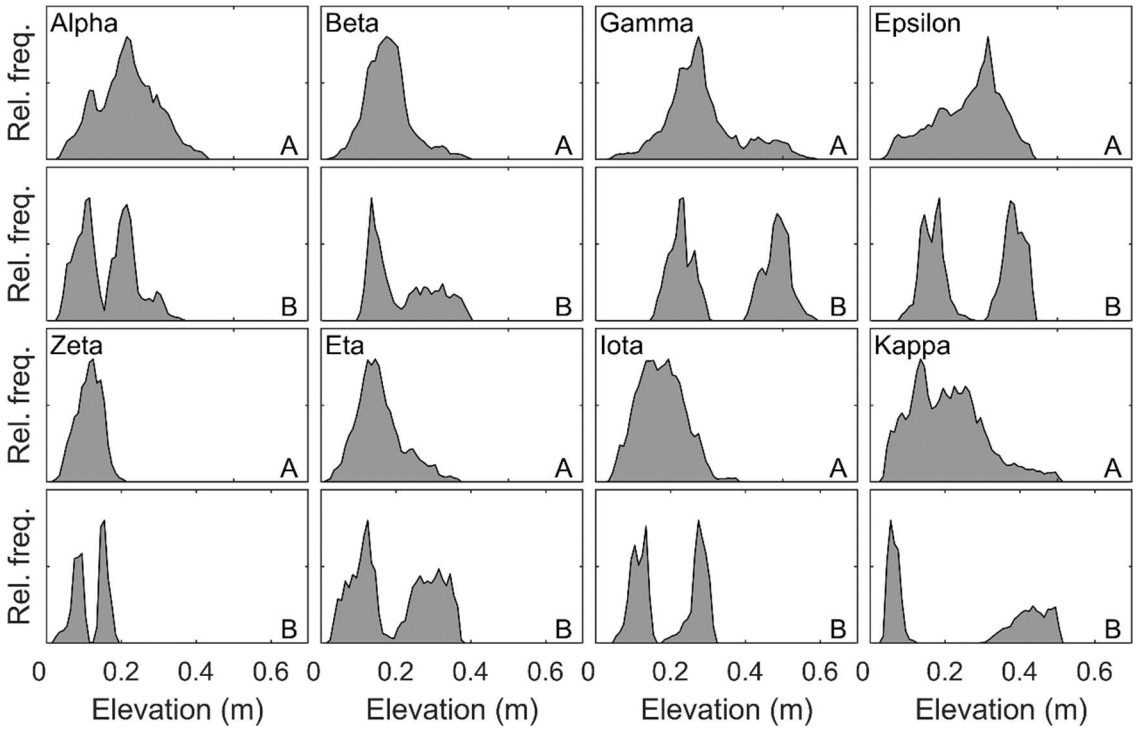

916

917

[Figure 5]

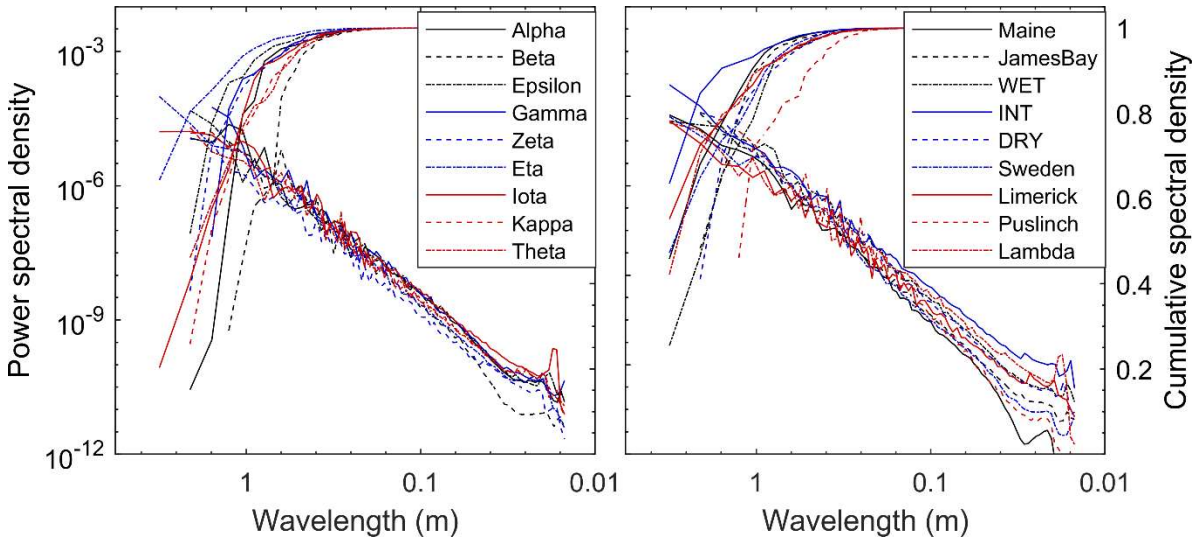
Power spectral density
10^{-3}
10^{-6}
10^{-9}
10^{-12}
1
0.1
0.01
Wavelength (m)
Alpha
Beta
Epsilon
Gamma
Zeta
Eta
Iota
Kappa
Theta
Maine
JamesBay
WET
INT
DRY
Sweden
Limerick
Puslinch
Lambda
Cumulative spectral density
1
0.8
0.6
0.4
0.2

921 [Figure 6]

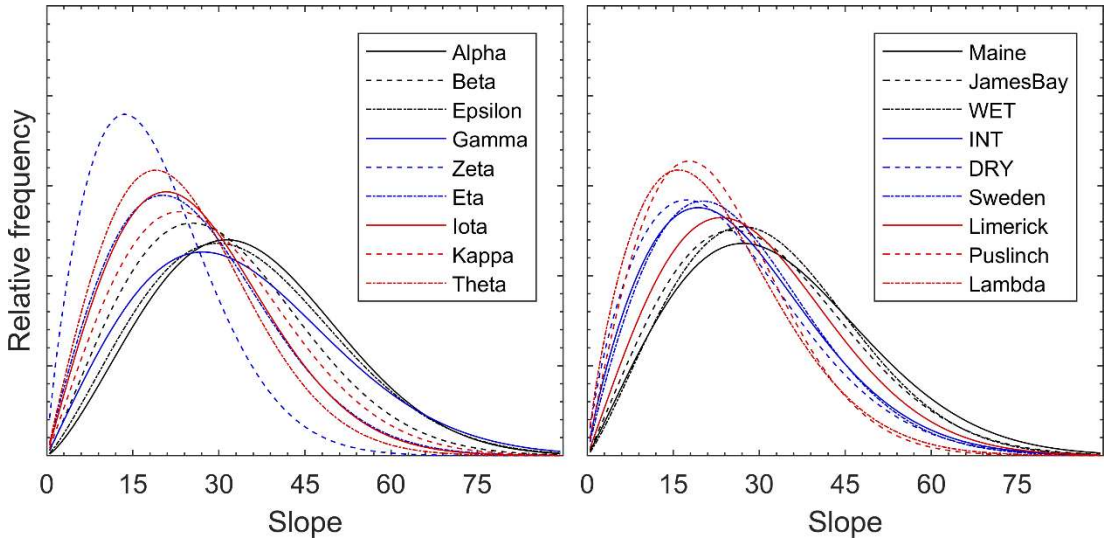

922

923

924

925 [Figure 7]

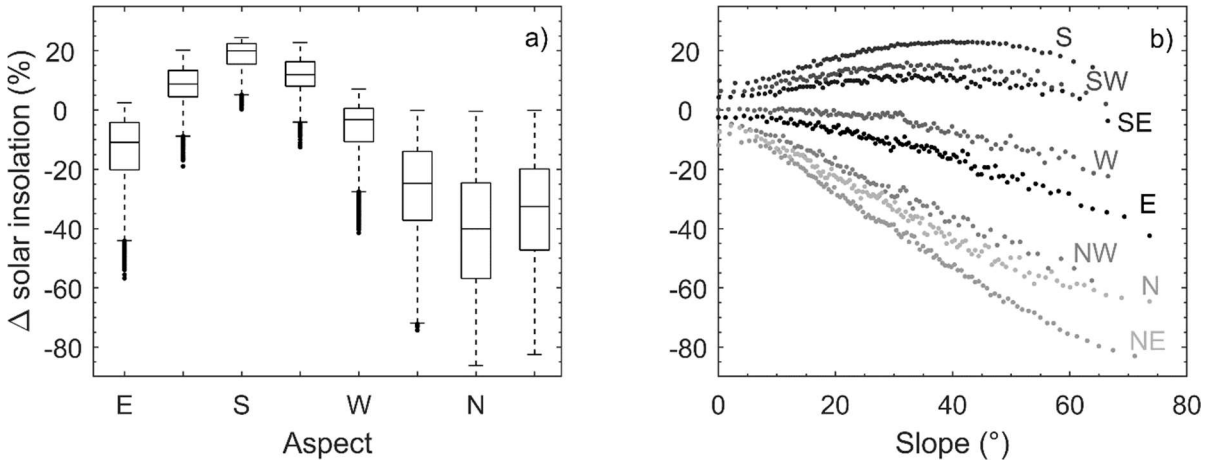

926

927

928

929 [Figure 8]

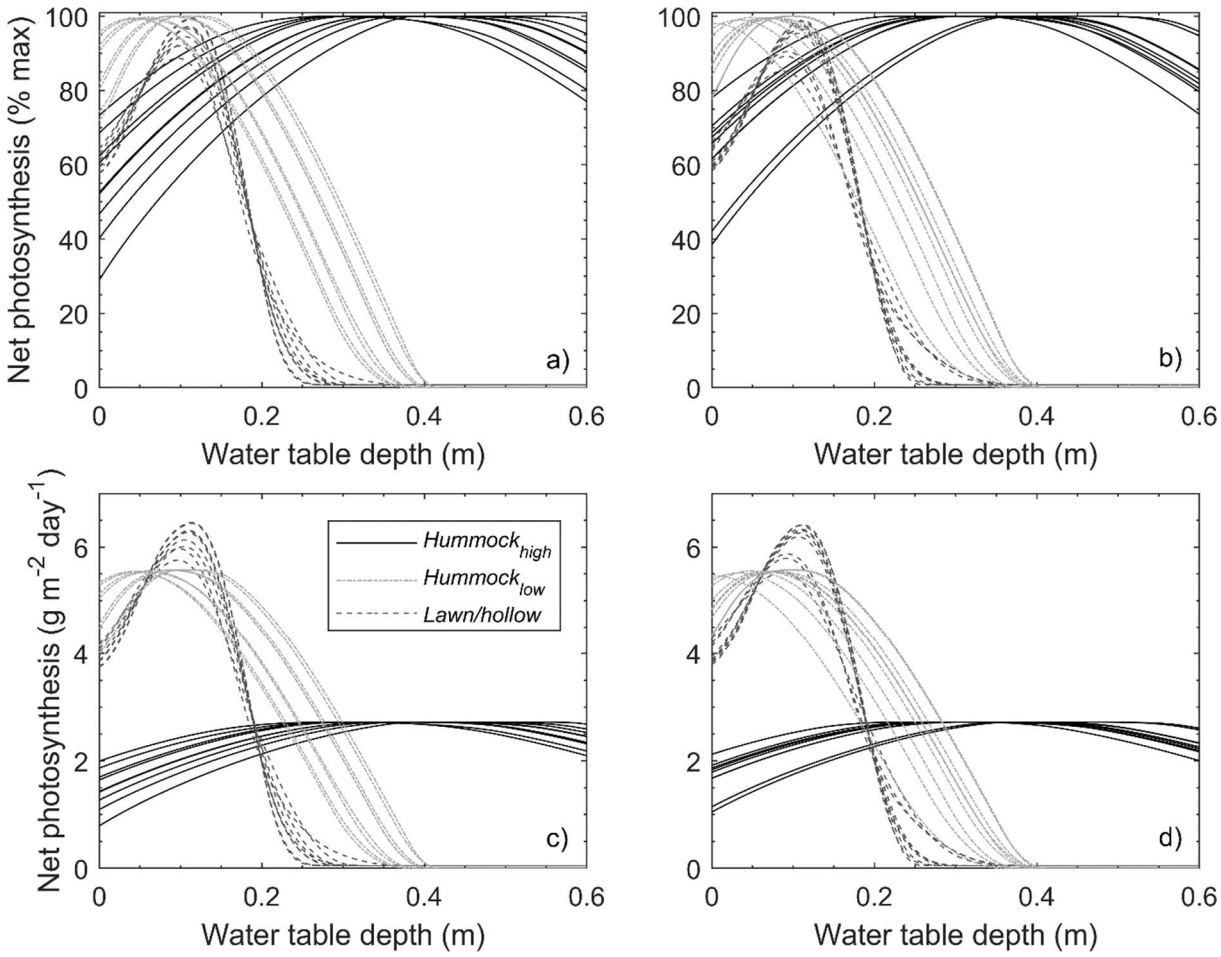

930

931
932

933 [Figure 9]

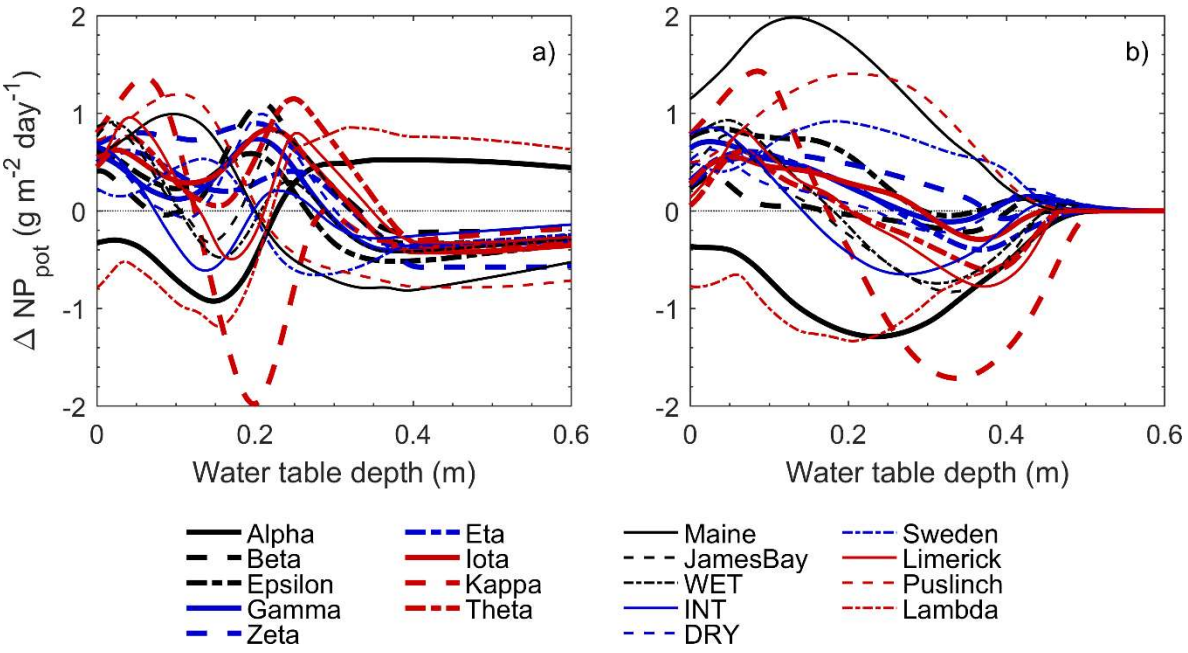

934

935

936 [Figure 10]

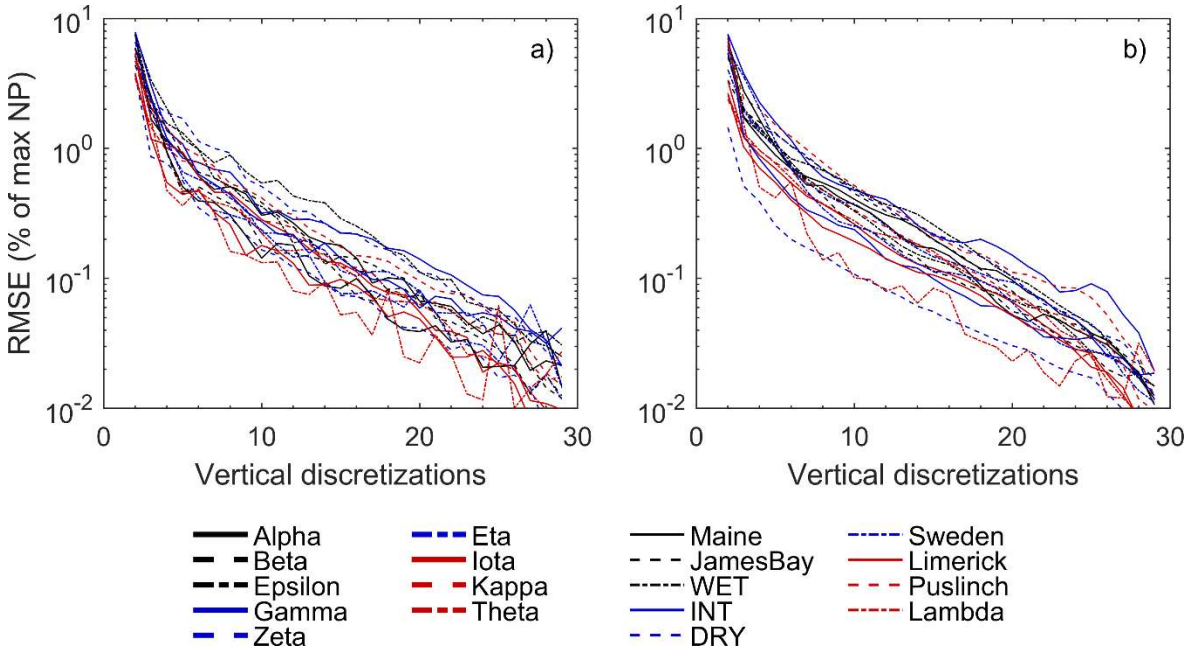

937

938